PCCP

Accepted Manuscript

ROYAL SOCIETY OF CHEMISTRY

www.rsc.org/pccp

PCCP

ARTICLE

Vibronic Bandshape of Absorption Spectra of Dibenzoylmethanatoboron Difluoride Derivatives: Analysis Based on Ab Initio Calculations

Received 00th January 20xx,

Accepted 00th January 20xx

DOI: 10.1039/x0xx00000x

www.rsc.org/

Pavel S. Rukin,[a] Alexandra Ya. Freidzon,*[a,c] Andrei V. Scherbinin,[b] Vyacheslav A. Sazhnikov,[a] Alexander A. Bagaturyants,[a,c] Michael V. Alfimov[a]

The nature of absorption bandshapes of dibenzoylmethanatoboron difluoride ($DBMBF_2$) dye substituted in *ortho-*, *meta-*, and *para*-positions of the phenyl ring is investigated using DFT and TDDFT with the range-separated hybrid CAM-B3LYP functional and the 6-311G(d,p) basis set. The solvent effects are taken into account within the polarized continuum model. The vibronic bandshape is simulated using time-dependent linear coupling model with vertical gradient approach through an original code. For flexible chromophores, the spectra of individual conformers are summed up with Boltzmann factors. It is shown that the long-wavelength absorption bandshape of $DBMBF_2$ derivatives is determined by three factors: the relative statistical weights of conformers with different electronic absorption patterns, the relative position and intensity of the second low-energy electronic transition, and the vibronic structure of individual electronic peaks. The latter is governed by the relationship between the hard vibrational modes, which contribute to the vibronic progression, and soft modes, which provide broadening of the peaks. The simulated spectra of the dyes in study are generally consistent with the available experimental data and explain the observed spectral features.

Introduction

The vibronic structure of absorption and emission spectra contains important information about molecular structure, vibrations, and dynamics on a femtosecond scale. However, this information can hardly be extracted directly from experimental data. Contributions of different factors to the overall spectrum can be properly analyzed using a computer simulation of vibronic spectra. Recently, both time-dependent and time-independent approaches to calculations of vibronic absorption and emission band shapes have been developed.[1–20] These approaches have been successfully applied to calculations of spectral band shapes for a large number of systems containing both inorganic[3–7] and organic[21–28] chromophores.

In optical chemical sensors, the absorption or emission bandshape can serve as an analytical signal responding to the interaction of the chromophore with analytes or environment.[29, 30] Therefore, the theoretical prediction of absorption or emission band shapes of various chromophores and their changes upon interaction with analytes is very important for the design and selection of materials for optical chemical sensors.[31]

The observed spectral features can originate not only from vibronic contributions but also from contributions of different electronic transitions as well. In addition, the spectral features of flexible chromophores contain contributions from different conformations. Therefore, in the case of flexible chromophores, their spectral features cannot be explained using purely vibronic models.

Difluoroboron β-diketonates show exceptional photophysical and photochemical properties.[32–35] In particular, these dyes exhibit high molar absorptivities and fluorescence quantum yields[36] and readily form exciplexes with aromatic compounds.[37–43]

A typical representative of this class of compounds, dibenzoylmethanatoboron difluoride ($DBMBF_2$), its derivatives, and complexes with some aromatic compounds were studied experimentally in detail[35, 37, 42] with the aim of using $DBMBF_2$ in optical chemical sensors for various aromatic compounds. The electronic absorption and fluorescence spectra of $DBMBF_2$ and its methyl, allyloxy, and alkoxysilyl derivatives were investigated in polar and nonpolar solvents,[35, 42, 44] and their fluorescence quantum yields, lifetimes, and vibronic structure were reported. All dyes exhibit a pronounced structure of absorption and emission bands.

[a] Photochemistry Center, Russian Academy of Sciences, ul. Novatorov 7a, Moscow, 119421 Russia. E-mail: freidzon.sanya@gmail.com
[b] Department of Chemistry, M.V. Lomonosov Moscow State University, Moscow 119991, Russia.
[c] National Research Nuclear University MEPhI, Kashirskoye shosse 31, Moscow, 115409, Russia.
† Electronic Supplementary Information (ESI) available. See
DOI: 10.1039/x0xx00000x

Unsubstituted $DBMBF_2$[44, 45] and its p-methyl derivative show similar structures of their vibronic spectra. The absorption spectrum of *p*-methyl-$DBMBF_2$ in the long-wavelength region exhibits pronounced peaks at 25900 and 27030, and a low intensity shoulder at 28330 cm^{-1}.

Replacing the methyl group by an O-containing substituent (allyloxy or propyloxysilyl group) leads to a bathochromic shift of the absorption bands due to the electron-donating nature of the substituent.[44] The spectra of allyloxy and propyloxysilyl derivatives are red-shifted by ~700 cm^{-1}. In addition, the spectra of their *m*-isomers are broadened as compared to *p*-isomers, and their shape is rather complicated. The spectra of *o*-isomers exhibit two distinct peaks at 25400 and 29200 cm^{-1}. The bathochromic shifts of the *o*- and *p*-isomers are similar, while the shift of the *m*-isomer is ~700 cm^{-1} smaller.

Previously, we calculated the geometrical structures and energies of electronic gas-phase transitions for absorption and emission of alkoxysilyl derivatives using DFT and TDDFT.[44] On the basis of these calculations, it was suggested that the above-mentioned spectral features of *p*-, *o*-, and *m*-substituted derivatives might be explained by an overlap of two electronic absorption bands. However, these calculations gave only the positions and oscillator strengths of the electronic transitions, and the relative intensities of individual transitions were not reproduced properly.

The 0–0 transition energies and absorption and emission band shapes were calculated for a series of dioxaborine fluorophores by Chibani et al.[46] using TDDFT, PCM, and time-independent approaches to the vibronic spectral shape. Unlike the rigid dyes investigated in the literature,[46] the chromophore moiety in substituted $DBMBF_2$ dyes can adopt different conformations, which can absorb at different wavelengths. In addition, they have flexible substituents, which can affect the vibronic structure of the spectra and even give rise to some additional spectral features. The determination of the nature of individual peaks and their spectral broadening associated with a certain substituent in the spectra of such dyes solely from experimental data is problematic. Quantum chemical calculations can be helpful in this case.

This paper is dedicated to the theoretical interpretation of the absorption spectra of $DBMBF_2$ derivatives (in particular, the nature of their band shapes) using DFT for the ground-state structures, TDDFT for the excited states, and the displaced multi-mode harmonic oscillator approximation[47, 48] for the vibronic structure of the absorption spectra.

Note that the calculated vibronic structure may depend on the exchange-correlation functional used in the calculations. The applicability of several DFT functionals to simulations of absorption and emission band shapes was investigated in detail in the literature.[49, 50] It might be concluded from Refs. 49 and 50 that the B3LYP, CAM-B3LYP, and PBE0 functionals provide reasonable agreement with experimental vibronic shapes, depending on the specific type of compounds. However, it was found in Ref. 44 that the PBE0 functional poorly reproduces the oscillator strengths and relative positions of some peaks for $DBMBF_2$ derivatives. Therefore in this work we considered the use of only the B3LYP and CAM-B3LYP functionals.

Computational details

We studied $DBMBF_2$ and its derivatives shown in Chart 1. The substituents were in the *ortho,- meta,-* or *para*-position of one benzene ring. *Ortho*- and *meta*-isomers exist in two types of conformations: (1) with the substituent directed toward the BF_2 group (type ***a***) and (2) with the substituent directed toward CH of the diketonate fragment (type ***b***). These two types of conformers can have noticeably different dipole moments and, therefore, different energies and intensities of electronic transitions. Hence, these conformers were considered individually.

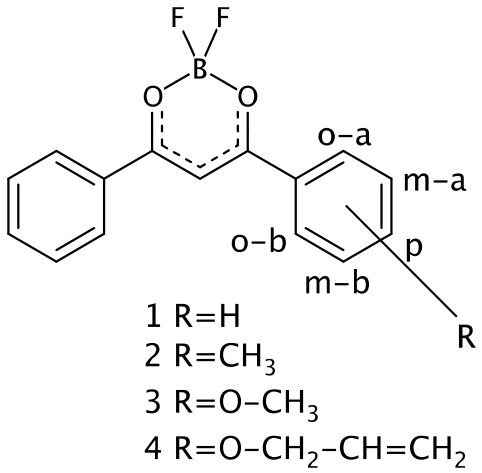

Chart 1. Chemical structure of the studied dyes.

Full geometry optimization was performed by DFT (CAM-B3LYP/6-311G(d,p) and B3LYP/6-311G(d,p)) with Grimme's dispersion correction.[51, 52]. Vertical absorption spectra were calculated by TDDFT with the same functionals and basis set. The bulk solvent (tetrahydrofuran) effect was included through the continuum solvation model SMD based on the quantum mechanical charge density of a solute molecule interacting with a continuum description of the solvent (PCM SMD).[53] The calculations were performed using the GAMESS-US package.[54]

For the vibronic structure simulation, we used the time-domain formalism[47, 48] and the multi-mode harmonic oscillator model of the potential energy surfaces,[48, 55–67] with all necessary parameters taken from the first-principles calculations according to the general methodology developed in Refs. 1–5. In brief, the normalized absorption band shape of each electronic transition is defined by the line shape function $I(\Omega)$, which is calculated as the Fourier transform of the generating function,

$$I(\Omega) = \frac{1}{2\pi}\int_{-\infty}^{\infty} G(t)e^{-i\Omega t}dt \qquad (1)$$

$$G(t)=\exp\left[\frac{it\left(\varepsilon_b^0-\varepsilon_a^0\right)}{\hbar}\right]\prod_j\exp\left[-S_j\left\{\coth\frac{\hbar\Omega_j}{2kT}\left(1-\cos\Omega_j t\right)-i\cdot\sin\Omega_j t\right\}\right] \quad (2)$$

Here, $\varepsilon_b^0-\varepsilon_a^0$ is the purely electronic («zero-phonon») $a\rightarrow b$ transition energy, Ω_j are the harmonic vibration frequencies, T is temperature (hereafter, T = 298 K in all vibronic structure simulations), and ħ and k are the Planck and Boltzmann constants, respectively.

$$S_j=\Omega_j\left(\Delta Q_j\right)^2/2\hbar \quad (3)$$

are the per-mode dimensionless Huang–Rhys (HR) parameters (or coupling strengths), with ΔQ_j being the harmonic potential energy minima shifts expressed in mass-weighted normal displacements.* The vibronic model parameters in Eqn (2) are found from the calculations of the ground state Hessian, the single-point excited state energy, and the gradient at the ground-state minimum configuration.

We assume that the overall absorption spectrum of the dye is a Boltzmann weighted sum of spectra of each conformer (*i*), which, in their turn, may consist of several bands. The area of each absorption band is normalized to the oscillator strength f_{ab}^i of the corresponding electronic transition $a\rightarrow b$

$$I^i(\Omega)=\sum_b f_{ab}^i I_{ab}^i(\Omega) \quad (4)$$

while the intensity distribution (vibronic structure) of each band is described by the respective line shape function $I_{ab}^i(\Omega)$ given by Eqns (1) and (2). The total absorption spectrum is calculated as

$$I(\Omega)=\sum_i w_i\sum_b f_{ab}^i I_{ab}^i(\Omega)\,, \quad (5)$$

where

$$w_i=\exp(-\Delta E_i/kT)/\sum_j\exp(-\Delta E_j/kT) \quad (6)$$

is the fraction of conformer (*i*) in the equilibrium mixture (Boltzmann weight), ΔE_i being the ground state energy difference between conformer (*i*) and the lowest energy conformer. Once the total absorption spectrum of the dye is calculated from Eqn (4), it can be rigidly shifted and normalized in order to provide a suitable comparison with experimental absorption data.

The calculation of Hessians with a polarizable continuum environment requires a special consideration. By default, all the ground-state calculations with PCM are performed using the static dielectric constant of the solvent, which includes both its electronic (fast) and structural (slow) relaxation. It is known (see, for example, the literature[68, 69]) that electronic transitions are so fast that only the fast response of the environment should be taken into account through its fast component at an infinite frequency. The vibrational transitions are 10–1000 times slower than the electronic transitions and, therefore, the structural relaxation of the solvent can also play a role. To estimate the possible influence of structural relaxation on the calculated vibrational frequencies, we compared the oscillation period for the lowest frequency vibrations (typically, 20 cm^{-1} in the studied dyes, which corresponds to ~1.7 ps) with the dielectric relaxation time of THF (which varies from 4 to 25 ps at room temperature).[70, 71] The slowest molecular vibrations in this case are faster than the structural relaxation of the solvent. Therefore, the fast dielectric constant should be used for the calculation of the hessians.

Results and discussion

Ground State Properties and Conformations

Ortho- and *meta*-substituted isomers of $DBMBF_2$ may have two different orientations of the substituted phenyl rings, which give rise to different orientations and values of the dipole moment. As mentioned above, we denote them as type ***a*** (the substituent pointed toward the BF_2 moiety) and type ***b*** (the substituent pointed toward the CH group of the diketonate). Allyloxy and methoxy substituents rotate almost freely and adopt the best orientation for each conformation.

Figure 1 gives the relative energies and dipole moment vectors of the studied conformers. Dyes ***4o*** and ***3o*** prefer type ***b*** conformations, which are stabilized by intramolecular C–H…O hydrogen bonds. Dye ***2o*** prefers type ***a*** conformation, which minimizes the interatomic repulsion. Conformers of type ***a*** and ***b*** in dyes ***4m***, ***3m***, and ***2m*** are close in energy.

To assess the ease of the conformational transitions from type ***a*** to type ***b*** in ***4m*** and ***3m***, we estimated the rotation barrier through a relaxed scan along the torsion angle between the phenyl ring and its substituent. The obtained value of ~5 kcal/mol means that both conformers can easily transform into each other at room temperature.

* We note in passing that the time-domain formalism and, particularly, Eqn (2), were first invented by M. Lax in 1952 in the study of optical band shapes.[48] Soon after Lax's original work, essentially the same technique was applied to studying optical transitions between more general multi-dimensional harmonic potential surfaces,[55–57] and was also adopted in the theory of radiationless transitions.[57–61] During the following decades, Lax's original concept proved to be a very fruitful tool in these and various related fields.[47, 62–67]

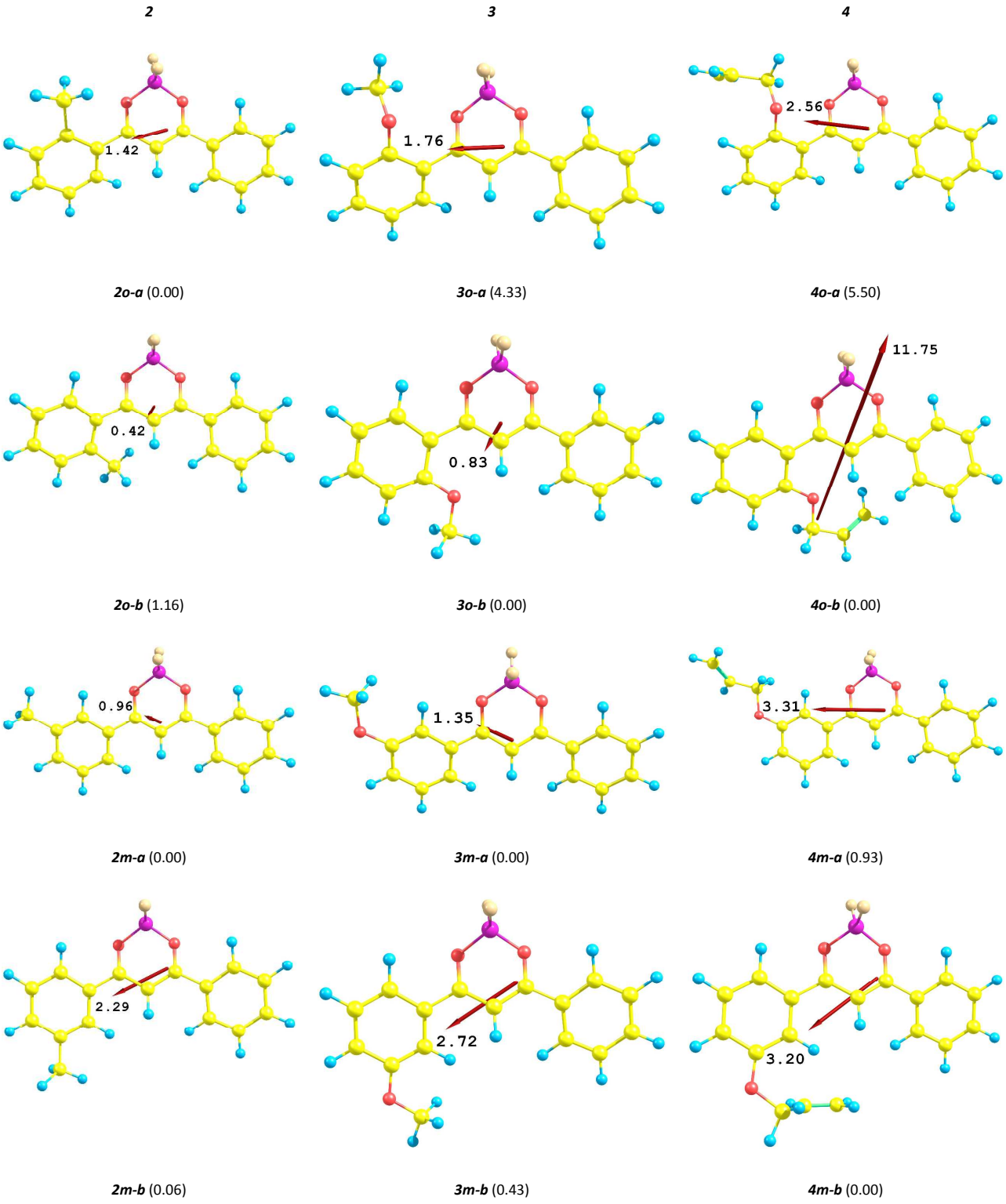

Figure 1. Dipole moments and relative energies in solvent (kcal/mol) of $DBMBF_2$ derivatives with respect to the most stable conformer.

Electronic Transitions

The vertical transition energies calculated by CAM-B3LYP are overestimated by ~3000 cm^{-1}, but the oscillator strengths and the relative positions of peaks (Table 1) are in a better agreement with experiment than those calculated at a PBE0/SVP level.[44] Similar calculations were performed with the B3LYP functional. The vertical transition energies agreed well with experiment, but, similarly to the literature,[44] the oscillator strengths for the *ortho*- and *meta*-isomers were incorrect (Table 2). Therefore, we decided to perform all further calculations with the CAM-B3LYP functional.

Our calculations show that there are two low-energy electronic transitions below 40000 cm^{-1} with the oscillator strengths higher than 0.3 for structures ***4o-b*** and ***3o-b*** and for both types of conformers of ***4m*** and ***3m***. Conformers ***4o-a*** and ***3o-a*** do not have second bright transition, in contrast with the experimental spectrum for ***4o***. Therefore, we can suggest that type **a** conformers of ***4o*** and ***3o*** do not contribute to the absorption spectra. This agrees with their high relative energies, which make them thermodynamically inaccessible.

At the same time, compounds ***2o***, ***2m***, ***2p***, ***4p***, and ***3p*** have only one bright transition in this range. Thus, we can suggest that it is the oxygen-containing substituent that causes the second peak to appear in the *ortho*- and *meta*-isomers.

Table 1. Calculated CAM-B3LYP/6-311G(d,p) vertical transition energies and oscillator strengths of $DBMBF_2$ derivatives.

Derivative	Transition energy, cm^{-1}		Energy difference, cm^{-1}	Oscillator strength	
	1st	2nd		1st	2nd
2o-a	31357	35994	4637	0.93	0.02
2o-b	31413	36010	4597	0.90	0.07
2m-a	30945	35760	4815	0.99	0.08
2m-b	31042	35470	4428	1.00	0.02
2p	30478	37180	6702	1.09	0.03
3o-a	32026	35647	3621	0.90	0.03
3o-b	29332	33857	4524	0.73	0.34
3m-a	29873	33149	3274	0.67	0.40
3m-b	30421	32663	2242	0.79	0.20
3p	29534	37470	7936	1.19	0.07
4o-a	32026	36107	4081	0.93	0.03
4o-b	29100	33931	4831	0.68	0.31
4m-a	29865	33204	3339	0.70	0.40
4m-b	30366	32221	2016	0.83	0.11
4p	29526	37478	7952	1.25	0.07

The orbitals of ***4o-a***, ***4m-a***, ***4m-b***, and ***4p*** isomers responsible for the first and second transitions are presented in Figure S1 of ESI. The same trend is observed in all the structures with methoxy substituent (***3***). The first transition is HOMO→LUMO, where HOMO is localized on the substituted phenyl ring, and LUMO is delocalized over the entire π system. The second transition is HOMO–1→LUMO, where HOMO–1 is delocalized. For methyl-substituted dye (***2***) and unsubstituted dye (***1***), the only bright transition is HOMO→LUMO, where HOMO and LUMO are both delocalized.

Table 2. Experimental[a] and calculated (B3LYP/6-311G(d,p)) absorption data of O-allyl $DBMBF_2$ derivatives.

	Experimental (in THF)			Calculated	
	λ, nm	*E*, cm^{-1}	ε, M^{-1} cm^{-1}	*E*, cm^{-1}	*f*
4o	394	25400	26820	25136	0.35
	380	26300			
	343	29200		29276	0.56
4m	385	26000	32680	24598	0.23
	370	27000			
	349	28700		28873	0.79
4p	397	25200	47380	26050	1.11
	384	26100		31776	0.02

[a] Ref. [44].

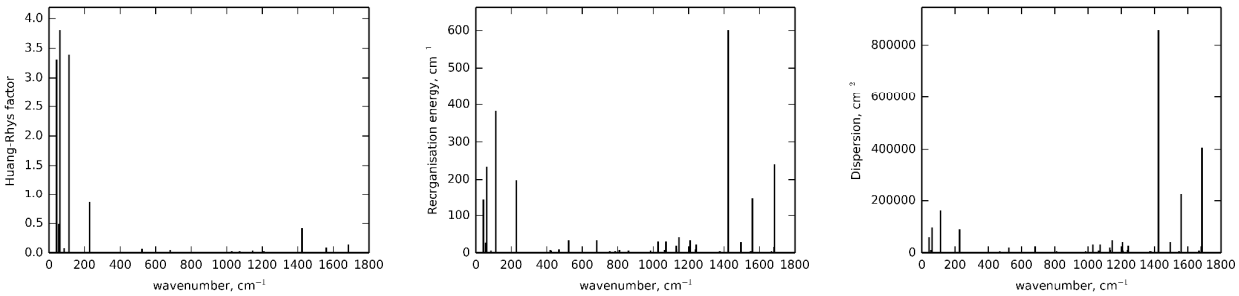

(a) (b) (c)

Figure 2. (a) Per-mode distributions of Huang–Rhys factors S_i; (b) partial contributions to the reorganization energy, Eqn (7); and (c) those to the dispersion of the absorption band of ***1***, Eqn (8).

The energy difference between the two lowest electronic transitions in ***4o-b*** and ***3o-b*** (4500 cm^{-1} and 4800 cm^{-1}, respectively) agree with the energy difference (3700 cm^{-1}) between the experimental first vibronic peak (25400 cm^{-1}) and the additional peak at 29100 cm^{-1}. The calculated oscillator strengths for these structures satisfactorily correlate with the experimental intensities. The spectrum of ***2o-a*** exhibits only one peak at 31357 cm^{-1}, and, as mentioned above, there is no additional peaks with the oscillator strength higher than 0.1.

Type ***a*** and type ***b*** geometries of ***4m*** and ***3m*** are separated by 1 kcal/mol, which indicates that these two conformers are present simultaneously in the equilibrium mixture, and their spectra should be summed with the corresponding Boltzmann weights (according to Eqns (5) and (6)) to give the total spectrum.

Two absorption bands in the available experimental spectra of ***4m*** and ***3m*** are not resolved. The calculated energies of the two lowest transitions are separated by 3200 cm^{-1} and 3300 cm^{-1} for ***3m-a*** and ***4m-a***, respectively, and 2200 cm^{-1} and 2000 cm^{-1} for ***3m-b*** and ***4m-b***. Dye ***2m*** gives only one bright transition in the UV–VIS region. Therefore, we may conclude that the second electronic peak results from the presence of the O-alkyl substituent in the *ortho*- or *meta*-positions of phenyl rings.

Para-substituted $DBMBF_2$ has no conformers, and its second electronic transition is forbidden. The first transition of ***2p*** is blue-shifted relative to ***3p*** and ***4p*** (Table 1), which agrees with the experiment.

Vibronic line broadening mechanism: «soft» and «hard» modes

To present a general view of the chromophore absorption spectrum, we start with the consideration of the vibronic structure of the individual electronic transition, which is described by the line shape function of Eqn (1). We try to explore the nature of the calculated vibronic structure using a simple and descriptive line broadening mechanism discussed, in particular, by M.D. Frank-Kamenetskii and A.V. Lukashin.[72] In brief, this mechanism is based on dividing all vibrations of the chromophore (and, possibly, of its environment) into two groups, «hard» (high-frequency) and «soft» (low-frequency) ones. The roles of these vibrations in the formation of the electronic transition band are qualitatively different. The hard vibrations are mainly responsible for the observed vibronic features, while the soft vibrations broaden these structures, making them less resolved. This broadening mechanism is often considered in theoretical studies of optical band shapes of various classes of molecular chromophores,[72–75] along with some other well-known mechanisms, e.g. homogeneous and inhomogeneous line broadening.[76–78]

In order to select the vibrations that are most strongly coupled with the electronic transition, it is instructive to consider the distribution of the calculated per-mode Huang–Rhys factors (coupling strengths) S_i (Eqn (3)) along with the corresponding partial contributions to the total reorganization energy and the total dispersion of the band:[3]

$$E_R = \sum_j S_j \hbar\Omega_j \qquad (7)$$

$$\sigma^2 = \sum_j S_j \Omega_j^2 \operatorname{cth}\frac{\hbar\Omega_j}{2kT} \qquad (8)$$

Note that the band dispersion parameter σ from Eqn (8) may be related to the full width at half maximum through the standard relation $\Gamma = 2\sqrt{2\ln 2}\cdot\sigma$.

A typical example is unsubstituted prototype dye ***1***, which has only one conformation and one bright electronic transition.

Figure 2 presents the HR factors of the absorption band of ***1***, per mode contributions to the reorganization energy, and those to the band dispersion. The pictures illustrate the increasing role of high-frequency (hard) modes in the reorganization energy and, especially, in the band dispersion (panels (b) and (c)), owing to the Ω_j and Ω_j^2 factors entering into Eqns (7) and (8), respectively, even though their Huang–Rhys factors are much smaller than those for the soft modes (panel (a)). According to the above mechanism, the soft modes can be chosen as the modes with large HR factors, while the important hard modes are those that give the largest contributions to the reorganization energy and band dispersion.

The largest Huang–Rhys factors, 3.31, 3.80, and 3.39, are from the soft modes with frequencies 43 cm^{-1}, 61 cm^{-1}, and 112 cm^{-1}, respectively. The hard modes with maximum Franck–Condon activity are at 1423 cm^{-1}, 1560 cm^{-1}, and 1684 cm^{-1} with

Huang–Rhys factors of 0.42, 0.09, and 0.14, respectively. The threshold frequency, below which the mode is considered as soft, and otherwise as hard, can be chosen at 250 cm^{-1} for this chromophore.

The generating function of Eqn (2) consists of individual factors for each normal mode and the purely electronic frequency multiplier. Apart from the last multiplier, all others can be grouped into two factors, incorporating all the hard and all the soft vibrations:

$$G(t) = \exp\left[it\left(\varepsilon_b^0 - \varepsilon_a^0\right)/\hbar\right] \cdot \overline{G}_{\text{hard}}(t) \cdot \overline{G}_{\text{soft}}(t) \quad (9)$$

According to the well-known properties of the Fourier transform, the corresponding absorption spectrum, Eqn (1), is the convolution of spectra originated from the soft and hard vibrations treated separately, additionally shifted by $\Omega_0 = \left(\varepsilon_b^0 - \varepsilon_a^0\right)/\hbar$ from the origin:

$$I(\Omega) = \int \overline{I}_{\text{hard}}(\Omega') \cdot \overline{I}_{\text{soft}}(\Omega - \Omega_0 - \Omega') d\Omega' \quad (10)$$

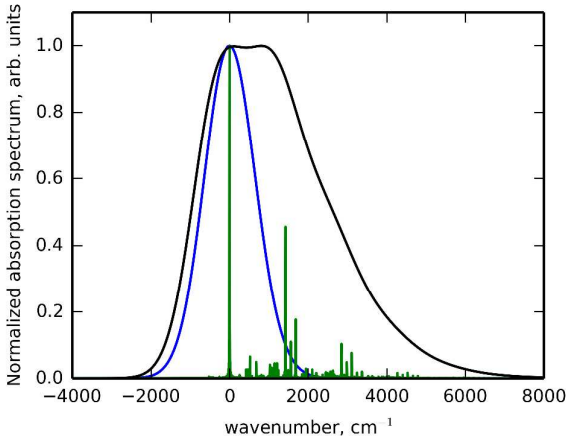

Figure 3. Calculated absorption spectrum of ***1***, $I(\Omega)$ (black) deconvoluted into the soft $\overline{I}_{\text{soft}}$ (blue) and hard $\overline{I}_{\text{hard}}$ (green) components according to Eqn (9). For clarity, the origin coincides with the 0-0 transition.

The simulated spectrum of ***1*** is presented in Figure 3. There are also individual spectra of hard and soft modes according to Eqn (10). The calculated absorption spectrum of hard modes consists of a series of discrete «sticks», whereas the soft mode spectrum is smooth and structureless. Therefore, the integral over Ω' in Eqn (10) is essentially reduced to a discrete sum over all the sticks of $\overline{I}_{\text{hard}}$:

$$I(\Omega) = \sum_{\Omega'} \overline{I}_{\text{hard}}(\Omega') \cdot \overline{I}_{\text{soft}}(\Omega - \Omega_0 - \Omega') \quad (11)$$

with the stick positions given by $\Omega' = \sum_{j \in \text{hard}} \Omega_j \Delta N_j$, where ΔN_j is the change in the occupation number of the *j*-th hard mode. Eqn (11) clearly indicates that each stick that corresponds to the hard mode spectrum is smeared with a continuous distribution $\overline{I}_{\text{soft}}$ (shown only for the 0-0 transition in Figure 3). The entire band, $I(\Omega)$, resembles a superposition of Franck–Condon progressions built from the most active hard modes (1423 cm^{-1}, 1560 cm^{-1}, 1684 cm^{-1}), though the corresponding vibronic structures are notably blurred.

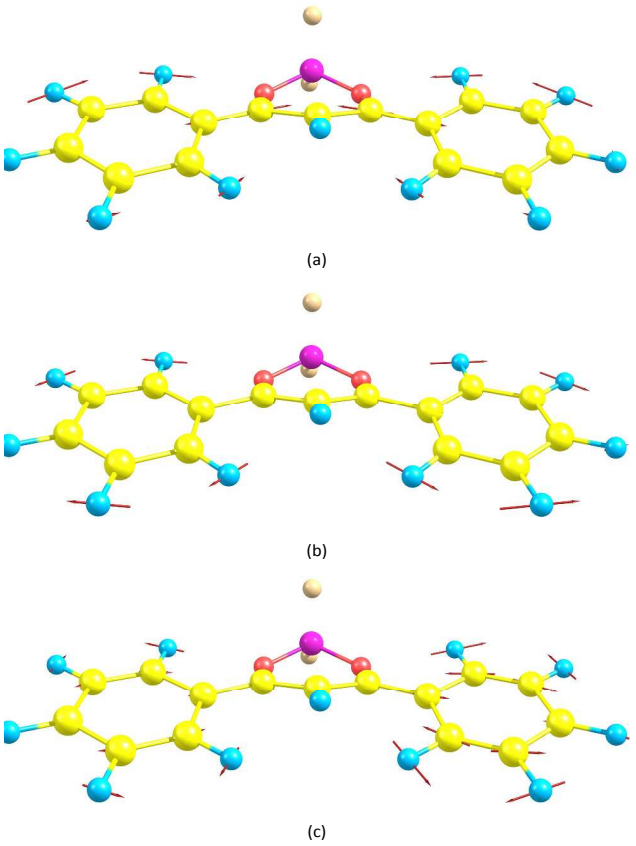

Figure 4. Atomic displacements of ***1*** corresponding to the modes at (a) 1423 cm^{-1}, (b) 1560 cm^{-1}, and (c) 1684 cm^{-1}.

Figure 4 demonstrates the atomic displacements of ***1*** corresponding to these hard modes. These are the characteristic in-plane deformations of the conjugated system (both phenyl rings and chelate cycle). On the other hand, the atomic displacement patterns corresponding to the most active soft modes mainly include the torsional and rocking vibrations of phenyl rings and the puckering of the chelate cycle (Figure 5).

Using the same approach, we have calculated and analyzed the absorption band shapes of the other $DBMBF_2$ derivatives under study, which are collected in ESI (Figures S2–S5). For almost all the structures, the most important vibrations are still the same as for ***1***. Upon substitution, these vibrations can shift to the lower frequencies or split into several modes with close frequencies due to the asymmetry brought by the substituents. The threshold frequency that determines a boundary between the soft and hard vibrations is nearly the same, ~250–260 cm^{-1} in all cases.

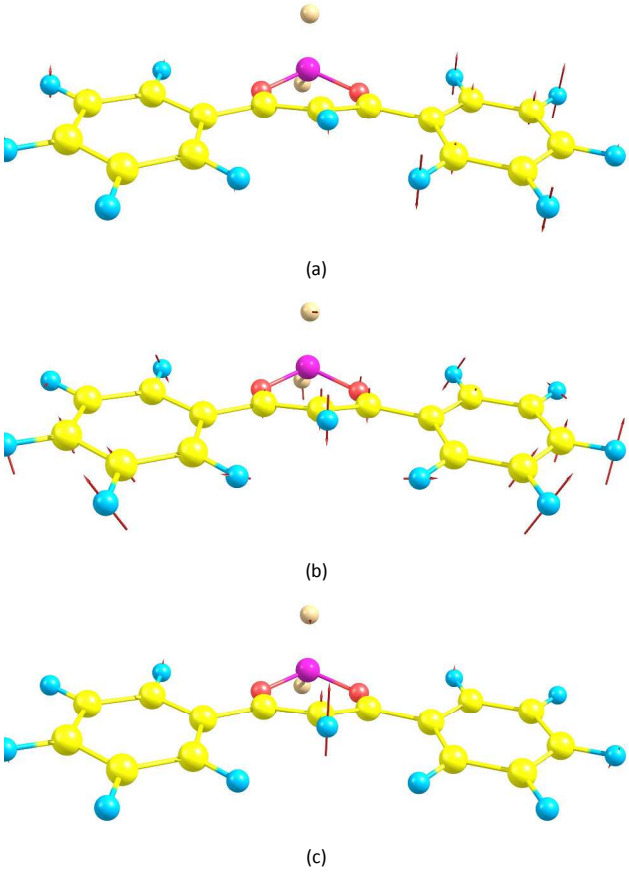

Figure 5. Atomic displacements of ***1*** corresponding to the modes at (a) 43 cm^{-1}, (b) 61 cm^{-1}, and (c) 112 cm^{-1}.

Let us discuss now the spectral resolution of the simulated absorption bands. It is natural to expect that the observed vibronic structures gradually disappear when the full width at half maximum of the soft mode spectrum,

$$\Gamma_{\text{soft}} = 2\sqrt{2\ln 2}\cdot\sigma_{\text{soft}},\ \sigma^2_{\text{soft}} = \sum_{j\in\text{soft}} S_j\Omega_j^2 \operatorname{cth}\frac{\hbar\Omega_j}{2kT},$$

becomes larger than the characteristic hard mode frequency $\langle\Omega_{\text{hard}}\rangle$ that gives the main progression. As an estimate for the latter, we use

$$\langle\Omega_{\text{hard}}\rangle = \sum_{i\in\text{hard}} S_i\Omega_i^2 \Big/ \sum_{i\in\text{hard}} S_i\Omega_i,$$

and introduce a dimensionless parameter $\gamma = \Gamma_{\text{soft}}/\langle\Omega_{\text{hard}}\rangle$ as a quantitative measure of the spectrum resolution. An inspection of the absorption band shapes calculated for various $DBMBF_2$ derivatives (see ESI, Table S1) shows that the estimated γ values correlate well with the expected trend in the spectral resolution: the simulated vibronic structure is more pronounced when γ decreases.

As an example, we present the absorption spectra corresponding to the first transition of the structures ***4o-b***, ***3o-b***, and ***2o-b*** (Figure 6).

One would expect that the soft mode spectrum becomes narrow due to the C–H…O contact between the oxygen of the substituent and diketonate hydrogen (***3o-b*** and ***4o-b***), and for ***3o-b*** due to the steric effect of the substituent that hampers out-of-plane vibration of the diketonate hydrogen.

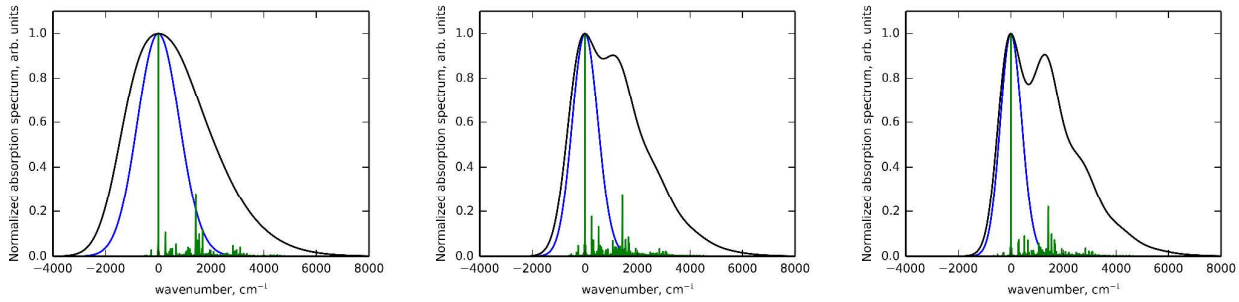

Figure 6. Calculated absorption spectra $I(\Omega)$ (black) of (a) ***2o-b***, (b) ***3o-b***, (c) ***4o-b*** deconvoluted into the soft $\bar{I}_{\text{soft}}$ (blue) and hard $\bar{I}_{\text{hard}}$ (green) contributions according to Eqn (9). See text for the explanation of γ.

Calculated vs. experimental absorption spectra

The case of one electronic transition and one stable conformer of the chromophore. Let us now compare the calculated absorption spectra with the experimental data for the structures that have only one low-energy conformer and only one intense electronic transition with a pronounced vibronic structure. As an example, the calculated and experimental spectra of ***1***, ***2p***, and ***4p*** are given in Figure 7. For convenience, the calculated spectra are red-shifted respectively by 3270 cm^{-1}, 3330 cm^{-1}, and 3350 cm^{-1}.

We can see that the calculated and the experimental spectra reasonably agree in their general shape, width, and resolution. In terms of the above-mentioned γ-based approach, the observed vibronic structures correspond to the γ~1 case (unfortunately, there is no sufficient experimental data for $DBMBF_2$ derivatives that might be related to more different γ

values). Though the calculated absorption spectra of ***1***, ***2p***, and ***4p*** do not reproduce quantitatively the relative height of the main vibronic peaks, they still follow the observed trend. Figure 7 also clearly demonstrates that the second group of sticks corresponds to the second vibronic peak. The greater the contribution of the main hard modes, the higher the second vibronic peak as compared to the first one. The calculated absorption spectra of ***2p*** and oxygen-containing derivatives ***3p*** and ***4p*** are compared in Figure S10 of ESI.

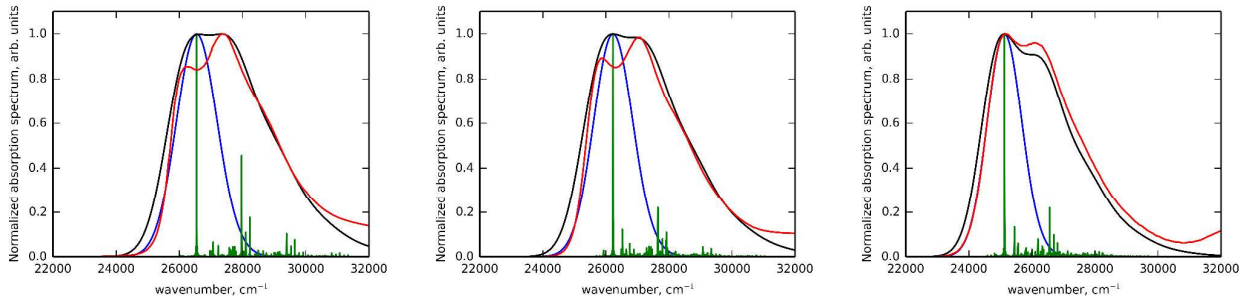

Figure 7. Experimental (red) and calculated absorption spectrum $I(\Omega)$ (black) of (a) ***1***, (b) ***2p***, (c) ***4p*** deconvoluted into the soft $\bar{I}_{\text{soft}}$ (blue) and hard $\bar{I}_{\text{hard}}$ (green) contributions according to Eqn (9). See text for the explanation of γ. The calculated spectra are shifted respectively by 3270 cm^{-1}, 3330 cm^{-1}, and 3350 cm^{-1} to match the experimental ones.

Overlap of two electronic transitions in one stable conformer of the chromophore. The spectrum of ***4o*** has two peaks separated by ~3800 cm^{-1} corresponding to different electronic transitions.[44] Our calculations give this difference as ~4800 cm^{-1}. We found only one low-energy conformer of ***4o*** (***4o-b***). Therefore, the absorption spectrum is a sum of two individual absorption bands, each having its own vibronic structure. Figure 8 shows the calculated and experimental spectra of ***4o-b***. The entire spectra of ***4o-b*** and ***3o-b*** are very similar and resemble the experimental spectrum (Figure S11, ESI).

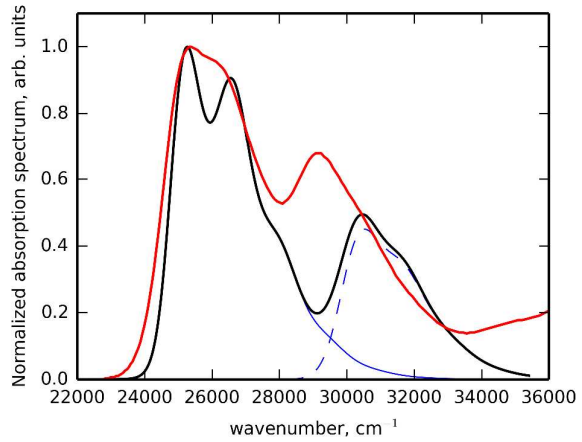

Figure 8. Calculated (black) and experimental[44] (red) absorption spectra of ***4o-b*** (the blue solid line corresponds to the first peak of ***4o-b***, the blue dash-dot line, to the second peak). The calculated spectrum is red-shifted to match the experimental one (by 2540 cm^{-1}).

Overlap of two electronic transitions in two stable conformers of the chromophore. Finally, we consider the most complicated spectrum of the chromophore ***4m*** that has two low-energy conformers with the ground state energy difference less than 1 kcal/mol (Figure 1). Each conformer exhibits two electronic transitions, each having its own vibronic structure. In addition, the energy separation between the two electronic transitions in the two conformers is also different (~3000 cm^{-1} in the ***a*** type conformer, and ~2000 cm^{-1} in the ***b*** type one). Therefore the overall spectrum is a Boltzmann-weighted sum of the spectra of each conformer. The calculated and experimental absorption spectra of ***4m*** are given in Figure 9.

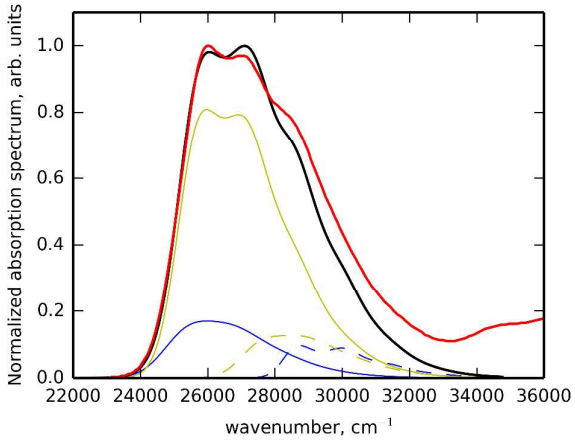

Figure 9. Calculated (black) and experimental[44] (red) absorption spectra of ***4m***. The blue lines are the first (solid) and second (dash-dot) peaks of ***4m-a***, the yellow lines are the first (solid) and second (dash-dot) peaks of ***4m-b***. The calculated spectrum is red-shifted to match the experimental one (3270 cm^{-1}).

The calculated spectra of ***2m***, ***3m***, and ***4m*** are compared in Figure S12 (ESI). The HR factors of individual peaks in the corresponding structures are quite similar (see Figure S3 in ESI). However, the band shape of ***3m*** differs substantially from that of ***4m***, because the ratio of the conformers in ***3m*** is not

the same as in ***4m***. This fact accounts for the different relative heights of individual peaks in the spectra.

Conclusions

Ab initio calculations have been performed for a series of electronic absorption spectra of flexible $DBMBF_2$ derivatives.

We demonstrate that the absorption band shape of $DBMBF_2$ derivatives is generally determined by the three factors: the relative statistical weights of conformers with different electronic absorption patterns, the relative position and intensity of the second electronic transition (which is due to the presence of oxygen-containing substituents), and the vibronic structure of individual electronic peaks. Taking into account all these factors simultaneously allows us to explain the nontrivial shape of absorption spectra of *o*- and *p*-O-allyl $DBMBF_2$ derivatives.

The vibronic structures of individual electronic transition bands of different $DBMBF_2$ derivatives are explored. For this purpose, the entire calculated electronic transition band is represented as a convolution of the two components, the hard mode spectrum, consisting of a series of discrete sticks, and a structureless soft mode spectrum, which effectively broadens the hard mode progressions. It is concluded that the observed vibronic structures of different $DBMBF_2$ derivatives are mainly due to the high-frequency modes corresponding to the characteristic in-plane vibrations of the diketonate moiety, while the broadening of these structures may originate from the out-of-plane low-frequency motions. A convenient quantitative measure of the resolution of the vibronic structures is proposed.

Acknowledgements

P.S.R., A.Ya.F., and A.A.B. thank the Russian Science Foundation, project No. 14-43-00052, for financial support. The calculations were performed using the facilities of the Joint Supercomputer Center, Russian Academy of Sciences, and NRNU MEPhI University cluster. We thank Dr. Yu.N. Kononevich (A.N. Nesmeyanov Institute of Organoelement Compounds and N.S. Enikolopov Institute of Synthetic Polymeric Materials, Russian Academy of Sciences) and V.N. Kopysov for the samples of $DBMBF_2$ derivatives, absorption spectra, and valuable discussions. We also thank the reviewers for carefully reading the manuscript and valuable suggestions.

1 T. Petrenko, F. J. Neese, *Chem. Phys*., 2007, **127**, 164319.
2 T. Petrenko, F. J. Neese, *Chem. Phys*., 2012, **137**, 234107.
3 P. V. Yurenev, M. K. Kretov, A. V. Scherbinin, N. F. Stepanov, *J. Phys. Chem. A*, 2010, **114**, 12804.
4 M. K. Kretov, I. M. Iskandarova, B. V. Potapkin, A.V. Scherbinin, A. M. Srivastava, N. F. Stepanov, *J. Lumin*., 2012, **132**, 2143–2150.
5 M. K. Kretov, A.V. Scherbinin, , N. F. Stepanov, *Russ. J. Phys. Chem. A*, 2013, **87** (2), 245–251.
6 A. Alkauskas, J. L. Lyons, D. Steiauf, C. G. Van de Walle, *Phys. Rev. Lett*., 2012, **109**, 267401.
7 Alkauskas, A. Buckley, B. B. Awschalom, D. D. Van de Walle, C. G. *New J. Phys*., 2014, **16**, 073026.
8 F. Santoro, *FCclasses, a Fortran code*, available at http://village.pi.iccom.cnr.it/software.
9 M. Biczysko, J. Bloino, F. Santoro, V. Barone, In *Computational Strategies for Spectroscopy: from Small Molecules to Nanosystems*; V. Barone, ed. Time-Independent Approaches to Simulate Electronic Spectra Lineshapes. From Small Molecules to Macrosystems; John Wiley & Sons, Inc. 2011, 361–446.
10 A. Lami, F. Santoro, In *Computational Strategies for Spectroscopy: from Small Molecules to Nanosystems*; V. Barone, ed. Time-Dependent Approaches to Calculation of Steady-State Vibronic Spectra: From Fully Quantum to Classical Approaches; John Wiley & Sons, Inc. 2011, 475–516.
11 A. Baiardi, J. Bloino, V. Barone, *J. Chem. Theory Comput*., 2013, **9**, 4097–4115.
12 V. Barone, M. Biczysko, J. Bloino, L. Carta, A. Pedone, *Comput. Theor. Chem*., 2014, **1037**, 35–48.
13 F. Santoro, A. Lami, R. Improta, V. Barone, *J. Chem. Phys*., 2007, **126**, 184102.
14 F. Santoro, R. Improta, A. Lami, J. Bloino V. Barone, *J. Chem. Phys*., 2007, **126**, 084509.
15 F. Santoro, A. Lami, R. Improta, J. Bloino, V. Barone, V. *J. Chem. Phys*., 2008, **128**, 224311.
16 V. Barone, J. Bloino, M. Biczysko and F. Santoro, *J. Chem. Theory Comput*., 2009, **5**, 540–554.
17 J. Bloino, M. Biczysko, F. Santoro and V. Barone, *J. Chem. Theory Comput*., 2010, **6**, 1256–1274.
18 E. Benassi, C. Cappelli, B. Carlotti, V. Barone, *Phys. Chem. Chem. Phys*., 2014, **16**, 26963-26973
19 J. Huh, R. Berger, *J. Phys. Conf. Ser*., 2012, **380**, 012019.
20 R. Borrelli, A. Capobianco, A. Peluso, *Can. J. Chem*., 2013, **91**, 495–504.
21 B. Minaev, Y. H. Wang, C. K. Wang, Y. Luo, H. Agren, *Spectrochim. Acta, Part A*, 2006, **65**, 308–323.
22 B. Minaev, H. Ågren, *Chem. Phys*., 2005, **315**, 215–239.
23 A. V. Bochenkova, L. H. Andersen, *Faraday Discuss*., 2013, **163**, 297.
24 V. Chashchikhin, E. Rykova, A. Scherbinin, A. Bagaturyants, *Int. J. Quant. Chem*., 2012, **112**, 3110–3118.
25 Y. Toker, D. B. Rahbek, B. Klærke, A. V. Bochenkova, L. H. Andersen, *Phys. Rev. Lett*., 2012, **109**, 128101.
26 A. V. Bochenkova, B. Klærke, D. B. Rahbek, J. Rajput, Y. Toker, L. H. Andersen, *Angew. Chem. Int. Ed*., 2014, **53**, 9797–9801.

27 A. V. Bochenkova, L. H. Andersen, In *Photophysics of Ionic Biochromophores, Physical Chemistry in Action*; S. Brondsted Nielsen and J.A. Wyer, eds. Photo-initiated Dynamics and Spectroscopy of the Deprotonated Green Fluorescent Protein Chromophore; Springer-Verlag, Berlin Heidelberg, 2013.
28 A.Ya. Freidzon, R. R. Valiev, A. A. Berezhnoy, *RSC Adv*., 2014, **4**, 42054–42065.
29 D. C. Dong and M. A. Winnik, *Photochem. Photobiol*., 1982, **35**, 17–21.
30 D. C. Dong and M. A. Winnik, *Can. J. Chem*., 1984, **62**, 2560–2565.
31 A. Bagaturyants M. Alfimov In *Chemical Sensors: Simulation and Modeling*, Vol. **4**: *Optical Sensors*; G. Korotcenkov Ed. Atomistic Simulation of Hierarchical Nanostructured Materials for Optical Chemical Sensing; Momentum Press, 2013, 1–38.
32 Y. L. Chow, C. I. Johansson, Y. -H. Zhang, R. Gautron, L. Yang, A. Rassat, S. -Z. Yang, *J. Phys. Org. Chem*., 1996, **9**, 7–16.
33 M. J. Mayoral, P. Ovejero, J. A. Campo, J. V. Heras, E. Oliveira, B. Pedras, C. Lodeiro, M. J. Cano, *Mater. Chem*., 2011, **21**, 1255–1263.
34 D.-J. Wang, Y.-F. Kang, L. Hu. Fan, Y.-J. Zheng, *J. Opt. Mater*., 2013, **36**, 357–361.
35 V. A. Sazhnikov, V. N. Kopysov, V. M. Aristarkhov, E. S. Shibneva, A. G. Mironchik, E. V. Fedorenko, M. V. Alfimov, *High Energy Chem*., 2011, **45** (6), 501–504.
36 K. Ono, K. Yoshikawa, Y. Tsuji, H. Yamaguchi, R. Uozumi, M. Tomura, K. Taga, K. Saito, *Tetrahedron*, 2007, **63**, 9354.
37 P. Valat, V. Wintgens, Y.L. Chow, J. Kossanyi, *Can. J. Chem*., 1995, **73**, 1902–1913.
38 Y. L. Chow, C. I. Johansson, *J. Phys. Chem*., 1995, **99**, 17558–17565.
39 Y. L. Chow, C. I. Johansson, *J. Phys. Chem*., 1995, **99**, 17566–17572.
40 Y. L. Chow, C. I. Johansson, Z.-L. Liu, *J. Phys. Chem*., 1996, **100**, 13381–13385.
41 Y. L. Chow, Z.-L. Liu, C. I. Johansson, J. Ishiyama, *Chem. Eur. J*., 2000, **6**, 2942–2947.
42 T.-T. Truong, V. Brenner, G. Ledoux, T.-H. Tran-Thi, *Photochem. Photobiol. Sci*., 2006, **5**, 686–697.
43 V. A. Sazhnikov, A. M. Muzafarov, V. N. Kopysov, V. M. Aristarkhov, Yu. N. Kononevich, I. B. Meshkov, N. V. Voronina, M. V. Alfimov, *Nanotechnol. Russ*., 2012, **7**, 6–14.
44 Yu. N. Kononevich, I. B. Meshkov, N. V. Voronina, N. M. Surin, V. A. Sazhnikov, A. A. Safonov, A. A. Bagaturyants, M. V. Alfimov, M. A. Muzafarov, *Heteroat. Chem*., 2013, **24**, 271–282.
45 G. V. Zakharova, A. K. Chibisov, V. A. Sazhnikov, Yu. N. Kononevich, M. A. Muzafarov M. V. Alfimov, *High Energy Chem*., 2013, **47** (6), 327–330.
46 S. Chibani, A. Charaf-Eddin, B. Mennucci, B. Le Guennic, D. Jacquemin, *J. Chem. Theory Comput*., 2014, **10**, 805−815.
47 E. J. Heller, *Acc. Chem. Res*., 1981, **14**, 368–375.
48 M. Lax*, J. Chem. Phys*., 1952, **20**, 1752–1760.
49 A. Charaf-Eddin, A. Planchat, B. Mennucci, C. Adamo, D. Jacquemin, *J. Chem. Theory Comput*., 2013, **9** (6), 2749−2760.
50 A. D. Laurent, D. Jacquemin, *Int. J. Quantum Chem*., 2013, **113**, 2019−2039
51 S. Grimme, J. Antony, S. Ehrlich, H. Krieg, *J. Chem. Phys*. 2010, **132**, 154104.
52 R. Peverati, K. K. Baldridge, *J. Chem. Theory Comput*., 2008, **4** (12), 2030–2048.
53 A. V. Marenich, C. J. Cramer, D. G. Truhlar, *J. Phys. Chem. B*, 2009, **113**, 6378.
54 M. W. Schmidt, K. K. Baldridge, J. A. Boatz, S. T. Elbert, M. S. Gordon, J. H. Jensen, S. Koseki, N. Matsunaga, K. A. Nguyen, S. Su, T. L. Windus, M. Dupuis, J. A. Montgomery *J. Comput. Chem*., 1993, **14**, 1347.
55 R.C. O'Rurke, *Phys. Rev*., 1953, **91**, 265.
56 H. D. Vasileff, Phys. Rev., 1954, 96, 603.
57 R. Kubo, Y. Toyozawa, *Prog. Theor. Phys*., 1955, **13**, 160
58 G. Rickayzen, *Proc. R. Soc. Lond. A*, 1957, **241**, 480-494
59 S. H. Lin, *J. Chem. Phys*., 1966, **44**, 3759
60 S. R. Englman, J. Jortner, *Mol. Phys*., 1970, **18**, 145.
61 K. F. Freed, J. Jortner, *J. Chem. Phys*., 1970, **52**, 6272
62 S. Mukamel, *Principles of Nonlinear Optics and Spectroscopy*. New York: Oxford University Press (1995).
63 Y. Toyozawa, *Optical Processes in Solids*. New York: Cambridge University Press (2003).
64 Y. Zhao, R. S. Knox, *J. Phys. Chem. A*, 2000, **104**, 7751.
65 S.-L. Shi, G.-Q. Li, S.-J. Xu, Y. Zhao, G.-H. Chen, *J. Phys. Chem. B*, 2006, **110**, 10475.
66 S.-J. Xu, G.-Q. Li, Y.-J. Wang, Y. Zhao, G.-H. Chen, D.-G. Zhao, J.-J. Zhu, H. Yang, D.-P. Yu, J.-N. Wang, *Appl. Phys. Lett*., 2006, **88**, 083123.
67 J. Gilmore, R. H. McKenzie, *J. Phys. Chem. A*, 2008, **112**, 2162.
68 J. Tomasi, B. Mennucci, R. Cammi, *Chem. Rev*., 2005, **105**, 2999-3093.
69 B. Mennucci, *WIREs Comput. Mol. Sci*., 2012, **2**, 386–404.
70 A. Chaudhari, P. Khirade, R. Singh, S. N. Helambe, N. K. Narain, S. C. Mehrotra, *J. Mol. Liquids*, 1999, **82**, 245-253.
71 G. K. Johri, R. Sharma, M. Johri, S. Saxena, *Proceedings of 14th International Conference on Dielectric Liquids* (ICDL 2002), Graz (Austria), July 7-12, 2002.
72 M. D Frank-Kamenetskii, A V Lukashin, *Sov. Phys. Usp*., 1975, **18** (6), 391–409.
73 C. K. Chan, J. B. Page, *J. Chem. Phys*., 1983, **79**, 5234–5250.
74 K. T. Schomacker, O. Bangcharoenpaurpong, P. M. Champion, *J. Chem. Phys*., 1984, **80**, 4701–4717.
75 P. O. J. Scherer, A. Seilmeier, W. Kaiser, *J. Chem. Phys*., 1985, **83**, 3948–3957.
76 K. T. Schomacker, P. M. Champion, *J. Chem. Phys*., 1986, **84**, 5314-5325.
77 M. K. Lawless, R.A. Mathies, *J. Chem. Phys*., 1992, **96**, 8037-8045.
78 A. B. Myers, *Annu. Rev. Phys. Chem*., 1998, **49**, 267–295.